Matter and Radiation at Extremes REVIEW scitation.org/journal/mre

Recent research progress of laser plasma interactions in Shenguang laser facilities

Cite as: Matter Radiat. Extremes 4, 055202 (2019); doi: 10.1063/1.5092446
Submitted: 11 February 2019 • Accepted: 5 May 2019 •
Published Online: 29 July 2019

Tao Gong,[1] Liang Hao,[2] Zhichao Li,[1] Dong Yang,[1,a)] Sanwei Li,[1] Xin Li,[2] Liang Guo,[1] Shiyang Zou,[2] Yaoyuan Liu,[3] Xiaohua Jiang,[1] Xiaoshi Peng,[1] Tao Xu,[1] Xiangming Liu,[1] Yulong Li,[1] Chunyang Zheng,[2] Hongbo Cai,[2] Zhanjun Liu,[2] Jian Zheng,[3] Zhebin Wang,[1] Qi Li,[1] Ping Li,[1] Rui Zhang,[1] Ying Zhang,[1] Fang Wang,[1] Deen Wang,[1] Feng Wang,[1] Shenye Liu,[1] Jiamin Yang,[1] Shaoen Jiang,[1] Baohan Zhang,[1] and Yongkun Ding[2,a)]

AFFILIATIONS

[1]Research Center of Laser Fusion, China Academy of Engineering Physics, Mianyang, Sichuan 621900, People's Republic of China
[2]Institute of Applied Physics and Computational Mathematics, Beijing 100088, People's Republic of China
[3]CAS Key Laboratory of Geospace Environment and Department of Engineering and Department of Engineering and Applied Physics, University of Science and Technology of China, Hefei, Anhui 230027, People's Republic of China

[a)]**Authors to whom correspondence should be addressed:** yangdong.caep@gmail.com and ding-yk@vip.sina.com

ABSTRACT

We report experimental research on laser plasma interaction (LPI) conducted in Shenguang laser facilities during the past ten years. The research generally consists of three phases: (1) developing platforms for LPI research in mm-scale plasma with limited drive energy, where both gasbag and gas-filled hohlraum targets are tested; (2) studying the effects of beam-smoothing techniques, such as continuous phase plate and polarization smoothing, on the suppression of LPI; and (3) exploring the factors affecting LPI in integrated implosion experiments, which include the laser intensity, gas-fill pressure, size of the laser-entrance hole, and interplay between different beam cones. Results obtained in each phase will be presented and discussed in detail.

I. INTRODUCTION

Lasers were proposed as a way to achieve inertial confinement fusion (ICF)[1] in the laboratory immediately after their invention.[2] By imploding a deuterium-tritium (D-T) fuel capsule with either lasers (direct drive) or laser-produced x-rays (indirect drive), a high-density core with a high-temperature "hotspot" inside is formed, which can ignite fusion reactions and produce an energy larger than that of the drive lasers. As a promising energy source, as well as an effective method for the laboratory exploration of physics under extreme high-energy-density conditions in astrophysical systems, laser-driven ICF has been intensively researched globally for several decades. Although fuel gain exceeding unit (i.e., the output fusion energy exceeding the energy deposited into the D-T fuel) was reported in recent indirect-drive experiments[3] performed at the National Ignition Facility (NIF) at Lawrence Livermore National Laboratory,[4] ignition has not yet been achieved. One of the critical issues preventing ignition is the impact of laser plasma interactions (LPI),[5] which exist in both direct drive and indirect drive. As an intense laser beam propagates through an underdense plasma, parametric instabilities such as stimulated Brillouin scatting (SBS) and stimulated Raman scattering (SRS) take place, leading to a significant loss in laser energy if left uncontrolled. Besides, SRS and another parametric instability, two-plasmon decay (TPD), can generate hot electrons with temperatures from tens to hundreds of keV, potentially degrading the implosion degree by preheating the fuel.[6] Additionally, when laser beams overlap in a flowing plasma, cross beam energy transfer (CBET)[7,8] can be excited, re-distributing the laser energy deposition and hence breaking the implosion symmetry.[9,10] As a result of these deleterious impacts, LPI is treated as one of the principal bounds on the available design space for achieving ignition[6] and great efforts have been made in the exploration of how it develops and how to control it.

In early hohlraum experiments performed on Shiva with 1.06-μm (1ω) lasers, about 1/3 and 1/2 of the incident laser energy was converted to Raman scattered light and hot electrons, respectively,[11]

leaving insufficient x-ray drive for fuel implosion. Since the growth rates (γ) of parametric instabilities are proportional to the square of the laser wavelength (λ) as $\gamma \propto I\lambda^2$, where I is the laser intensity, it was realized that shorter wavelength lasers were needed for the enhancement of energy coupling.[12] As expected, subsequent experiments with 0.53-μm (2ω) and 0.35-μm (3ω) lasers showed an evident reduction in the production of hot electrons and scattered light,[12] demonstrating the benefit of using shorter wavelength lasers. Therefore, 0.35-μm lasers were chosen as the drivers in large facilities for ICF research, such as Nova,[13,14] OMEGA,[15–17] and NIF[18] in the United States, LMJ[19,20] in France, and Shenguang laser facilities[21–23] in China. However, as drive power increases, LPI still plays a nontrivial role even in 0.35-μm lasers. For instance, SRS reflectivities of the order of 20% have been routinely detected from the inner cones of NIF high-gas-fill hohlraums,[24] beyond expectation.

To further control and suppress LPI, many strategies have been proposed and verified in experiments, which can generally be separated into two categories. One is to optimize the laser-beam quality via the use of smoothing techniques, such as continuous phase plate (CPP),[25] polarization smoothing (PS),[26] and smoothing by spectral dispersion (SSD).[27] The apparent reduction of scattered light has been observed in experiments with the application of these smoothing techniques.[6,28–33] The other category involves enhancing the Landau damping rates of the plasma waves by manipulating plasma conditions. For example, since the scattered light is positively related to plasma density,[31,34] near-vacuum hohlraums have been used to minimize the plasma density along the laser channel.[35] Moreover, due to the negative dependence of scattered light on plasma temperature,[31,32] the application of an external magnetic field has been proposed to increase plasma temperature.[36–38] Varying plasma ingredients is another way to enhance the Landau damping of an ion acoustic wave (IAW). By introducing a low-Z dopant into a mid- or high-Z plasma, SBS is largely reduced.[39,40] Although the Landau damping of an electron plasma wave is independent of plasma ingredients, a reduction of SRS has also been observed in experiments when a low-Z plasma is doped with a high-Z material.[41]

Although it seems that effective approaches have been found for controlling LPI, the quantitative prediction of LPI is still very challenging, due not only to its sensitive dependence on laser and plasma parameters but also to the potential occurrence of saturation processes. When $k\lambda_D \ll 1$ (with k and λ_D being the wave number of the electrostatic wave and the Debye length, respectively), wave-wave nonlinearities such as the Langmuir decay instability (LDI),[42,43] two-ion decay (TID),[44,45] and other effects[46–51] may take place, dissipating energy from the excited electrostatic wave and hence preventing LPI from further growth.[52] In contrast, when $k\lambda_D \geq 1$, kinetic saturation mechanisms, such as nonlinear frequency shifts due to particle trapping[53–56] dominate, causing a loss of resonance for LPI. In addition to single-beam LPI, many multi-beam processes have been identified,[57] which include CBET,[7–10] multi-beam SBS,[58,59] multi-beam SRS,[60,61] and multi-beam TPD.[62,63] These multi-beam LPI processes further increase the uncertainty in LPI predictions in ignition-scale experiments.

LPI has also been experimentally researched for more than two decades in China, primarily within the context of indirect-drive ICF. However, due to limitations in drive energy, early experiments were mainly limited to small-scale plasmas, far from meeting the required ignition conditions. Specific research on LPI in large-scale (~mm) plasma began about ten years ago after the first operation of the ~2 kJ Shenguang-II laser facility (SG-II).[21] During this period, gasbag targets were primarily used in experiments. The open geometry of these targets facilitated plasma-parameter measurement using Thomson scattering. The next generation laser facility (SG-10 kJ)[22] was capable of delivering energy of up to ~10 kJ, providing a suitable platform for LPI research in both vacuum and gas-filled hohlraums. Although the drive energy was still insufficient for ignition, valuable results beneficial to laser and target design in later facilities were obtained from the scale-reduced targets. When the ~180 kJ Shenguang laser facility (SG-180 kJ)[23] was put into operation, plasma parameters much closer to ignition conditions were achieved. LPI experiments were routinely performed, in order to identify the factors affecting LPI and hence develop predictable hohlraum platforms for integrated implosion experiments. Results from these LPI experiments are also expected to play an important role in future ignition experiments in assessing levels of scattered light as well as further optimizing target design.

In this article, we report on the progress of LPI research in the Shenguang laser facilities in the past ten years. Generally, this type of research can be divided into three phases, according to their research objectives. In the first phase, great efforts were made to develop platforms for LPI research in large-scale (~mm) plasma with limited drive energy. Several key diagnostics were also developed during this phase, including the temporally resolved Thomson scattering and temporally and spectrally resolved backscattering diagnostic system. The second phase aimed to explore the effectiveness of different beam-smoothing techniques on suppressing LPI. Both the reduction of scattered light and the enhancement of radiation temperature demonstrated the benefits of using smoothing techniques. In the third phase, research focus was placed on the identification of factors affecting LPI in integrated implosion experiments. A step-by-step roadmap was proposed to achieve this goal, and several steps have already been completed. Based on the current knowledge and the necessity of future ignition experiments, further plans of LPI research have been conceived, which will also be introduced at the end of this article.

The article is arranged as follows. Section II introduces the platforms for LPI research in mm-scale plasma. Beam smoothing techniques for suppressing LPI are represented in Sec. III. Factors affecting LPI in integrated implosion experiments are discussed in Sec. IV. Finally, Sec. V draws a summary and briefly discusses future plans.

II. PLATFORMS FOR LPI RESEARCH IN mm-SCALE PLASMA

In indirect-drive ICF, laser beams must propagate through a large-scale (~mm) and hot (~keV) plasma before depositing their energy at the hohlraum wall.[1] It is in this relatively uniform plasma where LPI processes take place. Therefore, to study LPI under ignition-relevant conditions, creating a plasma both at a large scale and high temperature is of great importance. However, when drive energy is limited, it is difficult to achieve these two goals simultaneously. Usually, a trade-off needs to be made or a dedicated experiment designed.

The initial experiments[64,65] aimed at creating a mm-scale plasma were performed with gasbag targets on SG-II, which was capable of delivering eight heater beams with a total energy of 2 kJ at 3ω, as well

as an additional interaction beam with an energy of 1 kJ at 2ω. A typical experimental configuration is shown in Fig. 1. The gasbag was made of two 400-nm thick polyimide films glued to each side of a 400-μm thick Ti washer. The inner diameter of the Ti washer was 1.6 mm. When the gasbag was filled with ~0.4–0.8 atm of either neopentane (C_5H_{12}) or Xe gas, its size in the normal direction of the Ti washer was inflated to ~1 mm. This size was maintained until the gas was irradiated by the heater beams. Uniform target self-emission with a size of ~1 mm was observed using a temporally integrated x-ray pinhole camera (XPHC) (see Fig. 2) as well as by a temporally resolved x-ray frame camera (XFC) (not shown here), demonstrating the creation of a mm-scale plasma. Although SG-II was capable of delivering eight heater beams, only four of them were used, in order to protect optical elements from being damaged by the opposite laser beam in this open geometry. Each heater beam was operating at 3ω with an energy of ~260 J in a 1-ns-square pulse. With the additional interaction beam, which was operating at 2ω at ~1 kJ in a 1-ns-square pulse, a plasma temperature of up to 0.6 keV (1.8 keV) was achieved for the C_5H_{12} (Xe) gas. The temperature was measured with high

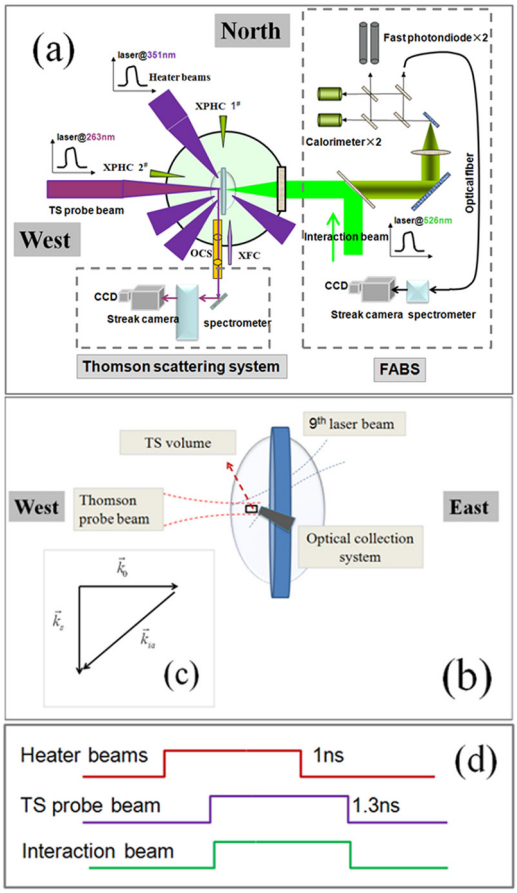

FIG. 1. (a) Schematic of experimental setup (top view), (b) geometry of Thomson scattering diagnostic (side view), (c) k-vector diagram of Thomson scattering diagnostic (top view), and (d) relative timings of laser beams in a typical gasbag experiment on SG-II. Reprinted with permission from Li *et al.*, Phys. Plasmas **19**, 062703 (2012). Copyright 2008 AIP Publishing LLC.[64]

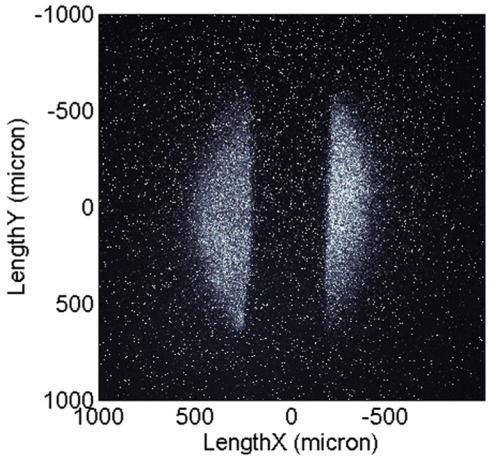

FIG. 2. Target self-emission in the photon energy above 2 keV measured by an x-ray pinhole camera (XPHC) in a typical C_5H_{12} gasbag experiment on SG-II. Reprinted with permission from Li *et al.*, Phys. Plasmas **19**, 062703 (2012). Copyright 2008 AIP Publishing LLC.[64]

precision (±15%) by the Thomson scattering diagnostic,[66] which took advantage of the open geometry of the target as well as the 4ω probe beam converted from one of the eight heater beams. Based on the known temperature, plasma density was inferred from the SRS spectra. The results indicated that a uniform plasma with a density of ~$0.1n_{c,2\omega}$ was formed in the interaction beam channel at an initial gas-fill pressure of 0.45 atm. Here, $n_{c,2\omega}$ denotes the critical density for the 2ω interaction beam. A similar gasbag filled with 0.8 atm of Xe gas was also tested on SG-10 kJ. When the target was heated by eight beams, each operating at 3ω with an energy of ~600 J in a 1-ns-square pulse, a mm-scale plasma with a temperature of ~1.6 keV and a density of ~$0.08n_{c,3\omega}$ ($n_{c,3\omega}$ being the critical density for the 3ω laser) was formed.[67] These plasma parameters are close to ignition-relevant conditions, making this gasbag a good platform for LPI research.

Exploiting this platform, the interaction of a 2ω laser with a mm-scale plasma was studied. The interaction beam was chosen to operate at 2ω rather than 3ω for two reasons. First, a 2ω laser is more likely to excite strong LPI than a 3ω laser because the growth rates of LPI processes are proportional to the laser wavelength. Second, the higher 1ω-to-2ω energy conversion efficiency leads to a higher intensity in the 2ω laser, making the excitation of LPI processes rather easier. Focused by an F/5.4 lens, this interaction beam was able to reach an intensity of 1.5×10^{15} W/cm^2. Moreover, to make full use of the plasma size, the interaction beam was incident on the target center with an angle of 45° relative to the vertical axis, as shown in Fig. 1(b). A backscattering diagnostic system [see Fig. 1(a)] was implemented on the interaction beam to measure the energy and the temporally resolved spectrum of the backscattered light.

The experimental results indicated that, although the plasma size was ~1 mm, SRS and SBS were actually excited in a limited region of ~0.2 mm. This limited region for LPI was demonstrated by the disruption behavior in the measured SRS spectra, indicating that the blast wave produced by the heater beams was passing through the SRS region.[64] Because the blast wave was followed by a rarefaction wave, as it was propagating into the target center, the overall plasma density

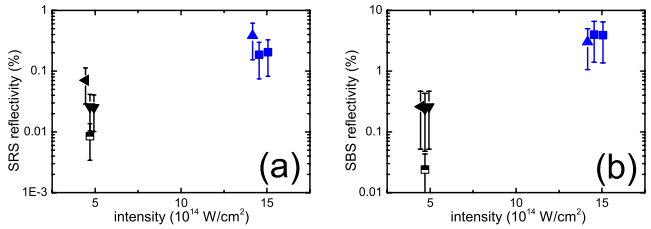

FIG. 3. Reflectivities of (a) SRS and (b) SBS as a function of laser intensity in gasbag experiments on SG-II. Triangles and squares are, respectively, for C_5H_{12} and Xe gasbags either with (black) or without (blue) beam smoothing. Reprinted with permission from Li *et al.*, Phys. Plasmas **19**, 062703 (2012). Copyright 2008 AIP Publishing LLC.[64]

decreased, and the density inhomogeneity increased. As a result, both SRS and SBS were at a low level (see Fig. 3), with reflectivities of ≤0.4% and ≤5%, respectively.

To overcome the quick rarefaction of the plasma, a specific gas-filled hohlraum was designed in subsequent experiments. Unlike the vertical placement in traditional experiments, the hohlraum axis in this specific experiment was placed along the 2ω interaction beam so that the interaction beam could penetrate the whole plasma enclosed by the hohlraum, as shown in Fig. 4. Due to the closed geometry of the hohlraum, all eight heater beams on SG-II were used to heat the plasma. They were injected into the hohlraum through two laser-entrance holes (LEHs) at the hohlraum waist (see Fig. 4).

With this experimental configuration, a uniform hot plasma with a scale-length much larger than that of the gasbag could be formed. Preliminary experiments were performed with a hohlraum of 0.8 mm in diameter and 2.2 mm in length. By filling the hohlraum with 0.4 atm of C_5H_{12}, this platform did show a much higher level of LPI than the gasbag, with the reflectivities of SBS and SRS being, respectively, ~10% and ~4% (see Fig. 5). These results indicated the formation of a large-scale plasma. By extending the duration of the interaction beam from ~1 ns to ~2.5 ns, while keeping its energy constant, a clear reduction in SBS and SRS reflectivities was observed, as shown in Fig. 5. This implied that, compared with the longer duration, the higher intensity of a laser played a more important role in LPI growth.

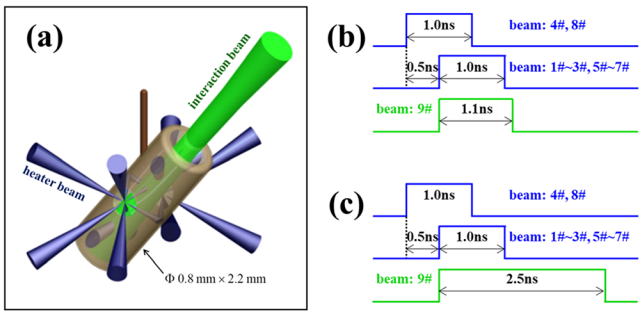

FIG. 4. (a) Experimental setup of a gas-filled hohlraum experiment on SG-II. The hohlraum is 0.8 mm in diameter and 2.2 mm in length, filled with 0.4 atm of C_5H_{12}. The diameter of the laser-entrance hole (LEH) at each end (waist) is 0.6 mm (0.45 mm). (b) Relative timings of heater beams (1#–8#) and the 1.1-ns interaction beam (9#). (c) Same as (b) except that the pulse duration of the interaction beam is extended to 2.5 ns.[64]

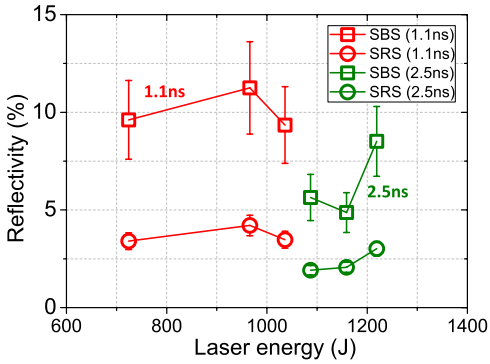

FIG. 5. Reflectivities of SBS (squares) and SRS (circles) as a function of laser energy in gas-filled hohlraum experiments on SG-II at different laser durations: 1.1 ns (red) and 2.5 ns (green).

Owing to the closed geometry, a Thomson scattering diagnostic was not applied in these preliminary experiments; as a result, the plasma temperature was not experimentally measured. The absence of temperature information further prevented the inference of density from the SRS spectrum. Therefore, efforts to characterize the plasma parameters need to be made so that further LPI experiments can be carried out on this platform in the future.

III. BEAM-SMOOTHING TECHNIQUES FOR SUPPRESSING LPI

The study on beam smoothing techniques was initially motivated by hohlraum energetics experiments performed on SG-10 kJ. After it was built, SG-10 kJ was used to explore hohlraum energetics with scale-reduced targets (compared with the targets in ignition experiments) by taking advantage of its capability to deliver eight laser beams with a maximum energy of ~10 kJ. In typical hohlraum energetics experiments, hohlraums with a diameter of 1 mm and a length of 2.1 mm were placed vertically at the target chamber center (TCC). The eight heater beams, each operating at 3ω with an energy of ~800 J in a 1-ns-square pulse, were injected into the hohlraum through the LEH at each end. However, the early experiments showed a low laser-to-hohlraum energy coupling efficiency (~70%), as well as a large shot-to-shot fluctuation in radiation temperature (±7 eV around 205 eV). One of the possible reasons was the high level of LPI caused by imperfections in the laser focal spot. As measured by later experiments, the focal spot was strongly nonuniform, meaning that about 40% of the laser energy was derived from intensities above 3×10^{15} W/cm^2, although the nominal average intensity was just about 4×10^{14} W/cm^2. As a result, up to 40% of SBS reflectivity was measured in vacuum-hohlraum experiments. These results motivated the quality improvement of laser focal spots with beam-smoothing techniques.

The first beam smoothing technique used on SG-10 kJ was the continuous phase plate (CPP). Its functionality was examined by specific experiments in which a single 3ω heater beam with an energy of ~100 J over 0.2 ns was fired onto a gold disk in each shot. The target self-emission in the energy range of the gold M-band, measured by an XPHC from the front side, was used to assess the laser intensity distribution at the target plane. Typical results with the incident laser operating at different conditions are displayed in Fig. 6. By assuming that the intensity of self-emission is proportional to the laser intensity

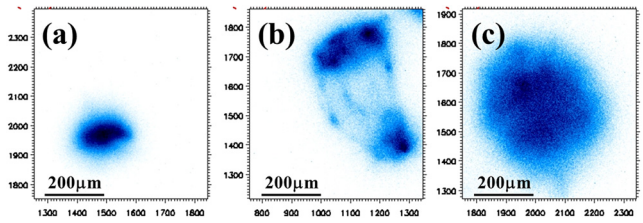

FIG. 6. Target self-emission in the energy range of gold M-band with different incident laser conditions: (a) focused without CPP, (b) defocused without CPP, and (c) focused with CPP.

during the 0.2-ns interaction, the laser intensity distribution can be inferred using the measured laser energy, as shown in Fig. 7. These results showed that, when the laser was focused by an F/5.4 lens onto the target without CPP, the focal spot was just ~150–300 μm in diameter and the intensity was nonuniformly distributed [see Fig. 6(a)]. As a consequence, ~70% of the laser energy was located above 1×10^{15} W/cm^2 (see Fig. 7). A large beam-to-beam difference was also observed in this focus mode. Of course, enlarging the spot by defocusing the laser beam can reduce the high-intensity component. However, the results indicated that the defocused mode did not significantly improve spot quality. When the laser was defocused onto the target in a diameter of ~500 μm, a footprint-like spot with a weak center surrounded by strong edges was observed, as shown in Fig. 6(b). As a result, ~50% of the laser energy was still located above 1×10^{15} W/cm^2. In contrast, after a Φ500 μm CPP (forming a focal spot of 500 μm in diameter) was applied, a much more uniform spot was obtained [see Fig. 6(c)], leaving ≤10% of the laser energy located above 1×10^{15} W/cm^2. Moreover, the beam-to-beam difference was also largely reduced. These results demonstrate the feasibility of CPP in improving focal spot quality. It should be noted that, due to radiation heating and plasma expansion, x-ray emission is unable to resolve the μm-scale speckles in the spot; consequently, the laser intensity distributions shown in Fig. 7 actually underestimate the high-intensity component, which will be discussed later.

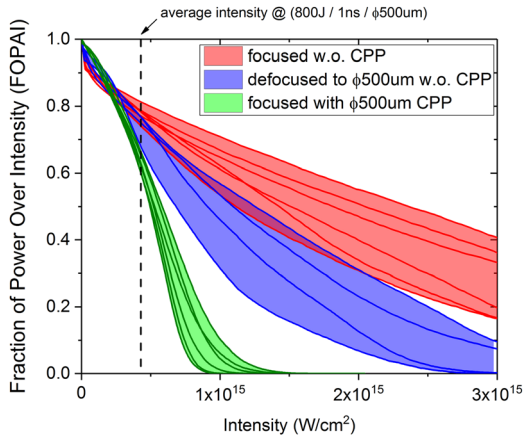

FIG. 7. Distributions of laser intensity inferred from the target self-emission with different incident laser conditions: focused without CPP (red), defocused without CPP (blue), and focused with CPP (green). The error bar represents the shot-to-shot fluctuation.

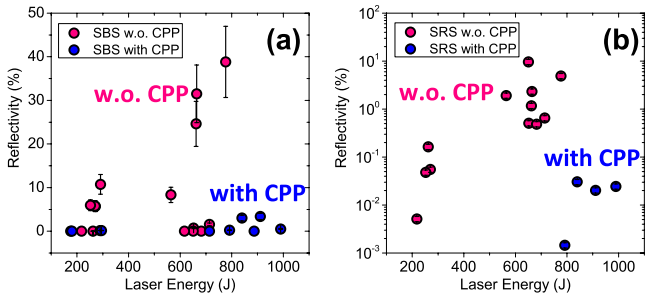

FIG. 8. Reflectivities of (a) SBS and (b) SRS as a function of laser energy in vacuum hohlraum experiments with (blue) and without (red) CPP.

The benefit of CPP to LPI and hohlraum energetics was then validated in vacuum hohlraum experiments on SG-10 kJ, by comparing the results with and without CPP added to all eight heater beams. As shown in Fig. 8, without CPP, maximum reflectivities of 40% and 10% were measured for SBS and SRS, respectively. In contrast, when CPP was added, SBS was reduced to ≤4%, while SRS was reduced to a negligible level. Additionally, the large shot-to-shot fluctuation in SBS and SRS reflectivities observed in experiments without CPP was also greatly mitigated when CPP was present. The benefit from CPP was verified too by the SRS spectra, as shown in Fig. 9. Due to the large high-intensity component in the laser spot when CPP was absent, the SRS threshold could easily be exceeded even in a low-density ($<0.1n_{c,3\omega}$) and inhomogeneous plasma. As a result, SRS spectra were spread over a wide spectral range (from 420 nm to 600 nm) and appeared shortly after the beginning of the laser pulse ($t = 0$ ns), as shown in Fig. 9(b). The large spatial region and the long temporal duration of the excitation of SRS might increase the uncertainty of its reflectivity, which could be an explanation for the large shot-to-shot fluctuation observed in Fig. 8(b). For comparison, the much more uniform laser spot, improved by CPP, limited SRS in a uniform, high-density ($\sim 0.12n_{c,3\omega}$) plasma. Therefore, the SRS spectra were narrowed around 560 nm and were present only at the end of the laser pulse [see Fig. 9(a)]. Thanks to the improvements in controlling LPI, the radiation temperature in the hohlraum not only increased by ~15 eV but also displayed a smaller shot-to-shot fluctuation, as shown in Fig. 10. As a result, the inferred laser-to-hohlraum energy coupling efficiency was enhanced from ~70% to ~90%, which would be beneficial for other applications such as implosion experiments. Large reductions in SBS and SRS reflectivities caused by CPP were

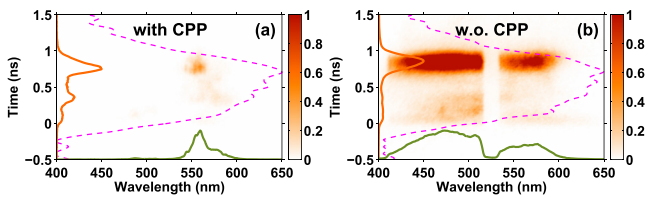

FIG. 9. Temporally resolved SRS spectra in vacuum hohlraum experiments (a) with and (b) without CPP. The absence of SRS spectra around 527 nm is due to the application of a notch filter in the measurement. The magenta dashed lines denote the corresponding laser pulse shapes in experiments.

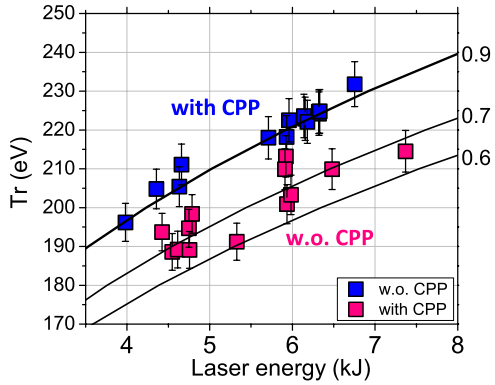

FIG. 10. Radiation temperature as a function of laser energy in vacuum hohlraum experiments with (blue) and without (red) CPP. The corresponding laser-to-hohlraum energy coupling efficiency is labeled right.

also observed in similar experiments with gas-filled (0.7 atm of C_5H_{12}) hohlraums, which is not shown here.

The improvement of focal spot quality caused by CPP was also analyzed on the subsequent larger laser facility of SG-180 kJ. Similar to NIF, the 48 beams of SG-180 kJ are injected into the vertically placed hohlraum at both ends through four cones of different angles relative to the hohlraum axis: 28.5° (8 beams), 35° (8 beams), 49.5° (16 beams), and 55° (16 beams). Each beam is able to deliver a maximum energy of 3.7 kJ in a 3-ns-square pulse at 3ω. Unlike the indirect method of characterizing spot quality by x-ray emission on SG-10 kJ, the laser spot on SG-180 kJ was directly measured via an optical approach. Due to the high spatial resolution (~1 μm) of this approach, the spot quality could be better characterized. As shown in Fig. 11(a), when CPP was removed, numerous intense speckles were observed in the focal spot. These speckles, with a transverse size of several microns, could not be resolved in the corresponding x-ray emission [see Fig. 11(c)]. A focal spot, generally reproducing the x-ray emission, was obtained by convoluting the optical spot with a point spread function (PSF) of 30 μm in full width at half maximum (FWHM), as shown in Fig. 11(b). This meant that a spatial resolution of 30 μm in FWHM would be introduced by radiation heating and plasma expansion.

With this high-resolution optical approach, focal spots with and without CPP were measured at the plane normal to the beam axis for two beams at each of the four cones. All of these eight beams

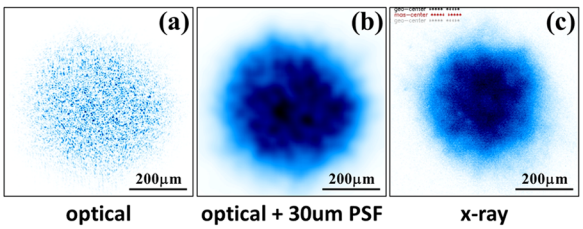

FIG. 11. (a) Optical focal spot measured on SG-180 kJ without CPP. (b) Focal spot obtained by convoluting (a) with a point spread function (PSF) of 30 μm in full width at half maximum (FWHM). (c) Focal spot measured by the x-ray emission on SG-180 kJ without CPP.

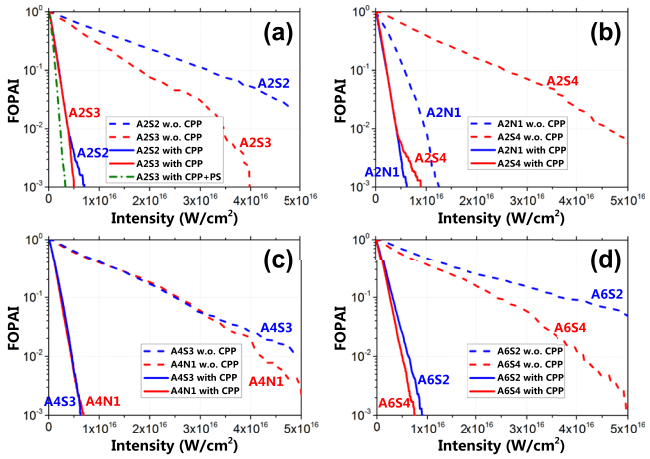

FIG. 12. Intensity distributions of focal spots with (solid) and without (dashed) CPP in different cones of beams: (a) 28.5°, (b) 35°, (c) 49.5°, and (d) 55°. The dash-dotted line in (a) represents the intensity distribution when additional polarization smoothing (PS) is applied.

are equipped with backscattering diagnostic systems. The intensity distributions inferred from these focal spots are displayed in Fig. 12. Similar to the results measured on SG-10 kJ, the application of CPP on SG-180 kJ also significantly improved focal spot quality by reducing the high-intensity component. In addition, the beam-to-beam difference of spot quality in the same cone was largely decreased after the application of CPP, which is beneficial to the radiation symmetry inside the hohlraum. As expected, a great reduction in SBS and SRS reflectivities was observed in early hohlraum experiments with CPP. Therefore, CPPs are routinely added to all 48 beams of SG-180 kJ. It should be noted that there is still a discernable difference in focal spot quality between beam A6S2 and beam A6S4 in the 55° cone after the application of CPP, which might lead to different SBS and SRS reflectivities between these two beams.

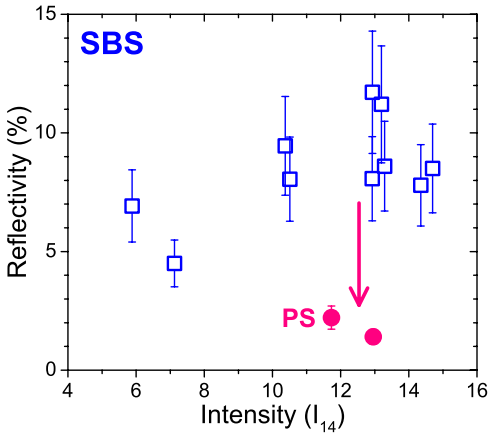

FIG. 13. SBS reflectivities with (solid) and without (open) PS measured in gas-filled hohlraum experiments on SG-180 kJ.

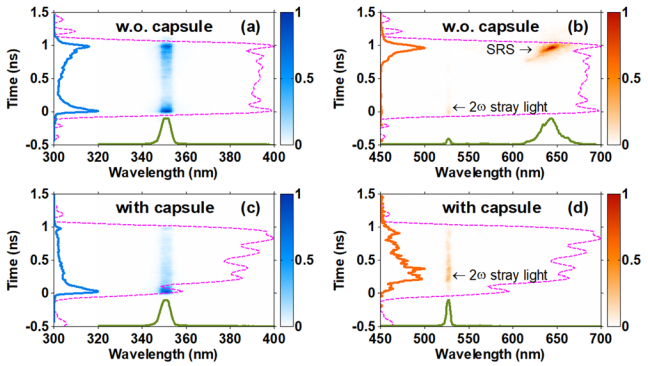

FIG. 14. Temporally resolved SBS intensity (left column) and SRS spectra (right column) without (top row) and with (bottom row) a surrogate capsule in a vacuum hohlraum on SG-10 kJ. The magenta dashed lines denote the corresponding laser pulse shapes in experiments.

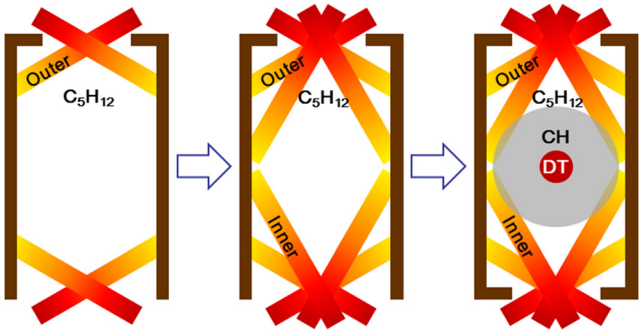

FIG. 15. Step-by-step roadmap of LPI research on SG-180 kJ.

Polarization smoothing (PS) is another effective technique for suppressing LPI. Its effect on laser focal spot quality was also studied using the optical approach. As shown in Fig. 12(a), PS further reduced the high-intensity component in the focal spot. This improvement greatly mitigated the growth of LPI; as a result, a dramatic reduction in SBS reflectivities from ~10% to ≤2% was observed when PS was applied, as presented in Fig. 13. Smoothing by spectral dispersion (SSD) has already been applied to the entire 48 beams on SG-180 kJ. Its effect on suppressing LPI will be studied in the near future.

IV. FACTORS AFFECTING LPI IN INTEGRATED IMPLOSION EXPERIMENTS

The ultimate goal of LPI research in laser indirect-drive ICF is to predict the hohlraum conditions so as to optimize the designs of lasers, hohlraums, and fuel capsules. To achieve this goal, LPI itself should be understandable and predictable. However, compared with the simple experiments specifically designed for LPI study, the integrated implosion experiments are much more complicated. LPI processes in these experiments can be affected by many factors, such as ablated plasma from the capsule, gas pressure in the hohlraum, the LEH size, and the interplay between lasers from different cones. The effects of ablated plasma from the capsule on LPI processes was observed in experiments on SG-10 kJ, where a vacuum hohlraum (1.1 mm in diameter and 2.0 mm in length) with and without a surrogate capsule placed at the center was irradiated by the eight beams from both ends. As shown in Fig. 14, the presence of the capsule largely reduced the intensities of SBS and SRS in the second half of the laser pulse, indicating that the plasma conditions inside the laser channel were gradually changed during the laser duration by ablated plasma from the capsule. However, the complicated, integrated experiments make it difficult to benchmark numerical simulations. For example, spectral analysis codes (HLIP[68] and S4P-1D[69]) in combination with a radiative hydrodynamic code (LARED-JC[70]) routinely overestimate the wavelength of SRS spectra in gas-filled hohlraum experiments in SG-180 kJ. The reason for

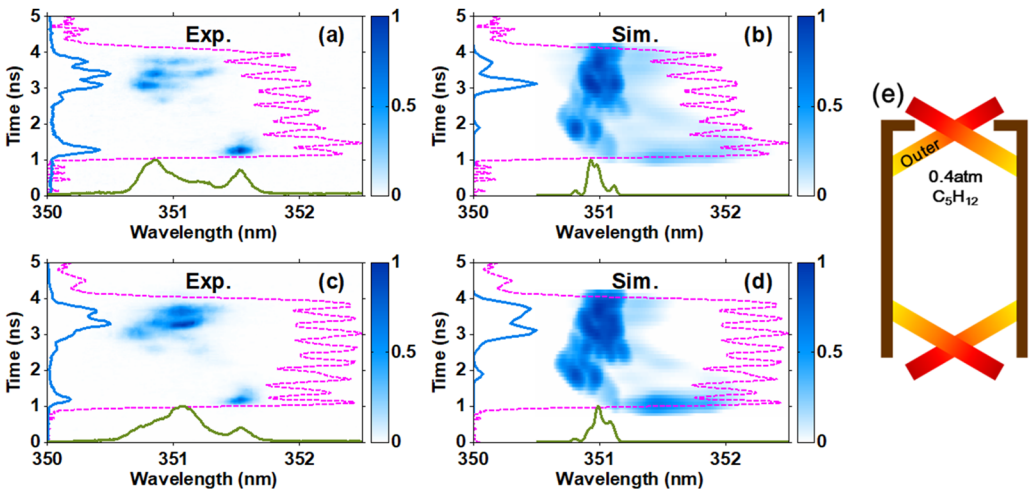

FIG. 16. (a), (c) Experimentally measured and (b), (d) simulated SBS spectra with interaction beam intensities of (a), (b) 6×10^{14} W/cm^2 and (c), (d) 1×10^{15} W/cm^2, respectively. The laser pulse shapes in the simulations are identical to the corresponding ones in experiments, as displayed by the magenta dashed lines. (e) The sketch of the experimental setup.

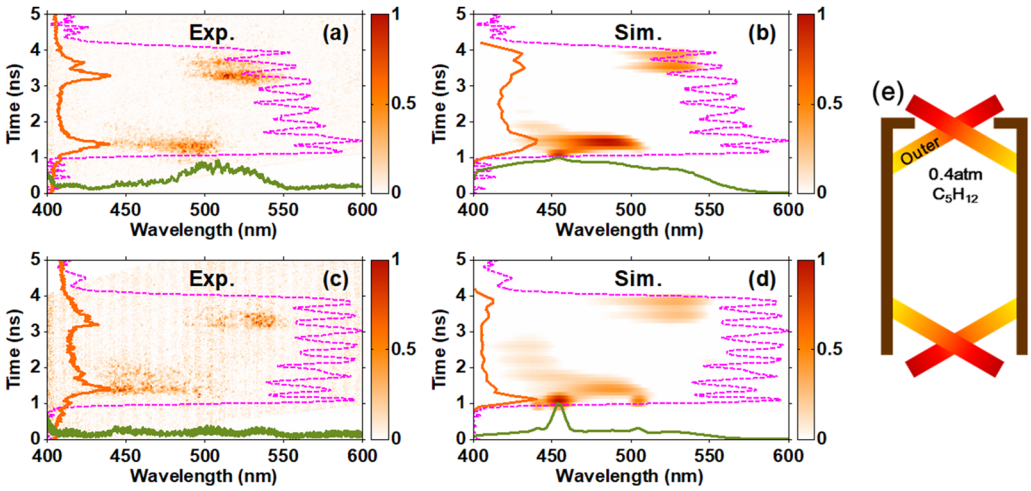

FIG. 17. (a), (c) Experimentally measured and (b), (d) simulated SRS spectra with interaction beam intensities of (a), (b) 6×10^{14} W/cm^2 and (c), (d) 1×10^{15} W/cm^2, respectively. The laser pulse shapes in the simulations are identical to the corresponding ones in experiments, as displayed by the magenta dashed lines. (e) The sketch of the experimental setup.

this inconsistency between simulation and experiment cannot be well identified in complicated integrated experiments.

Given the complexity of LPI processes in integrated experiments, a step-by-step roadmap has been proposed for SG-180 kJ to identify each of the factors affecting LPI, as presented in Fig. 15. This roadmap generally consists of three steps. In the first step, a simple experimental configuration is used. The fuel capsule is taken off and the LEH at one end of the hohlraum is removed. The gas-filled hohlraum is irradiated by 32 beams from the outer cones (49.5° and 55°). The dependence of LPI on laser intensity, gas pressure, and LEH size will be studied on this platform. Since the backscattering diagnostic systems are located in the lower hemisphere, the hohlraum will be flipped upside down when the effect of LEH size is studied. In the second step, the 16 beams from the inner cones (28.5° and 55°) are added to explore the interplay between the beams from different cones. The surrogate capsule will be introduced in the third step, so that the influence of ablated plasma from the capsule can be studied.

Following this roadmap, several large experiments have already been completed along with their corresponding numerical simulations. The hohlraums used in these experiments were 2.2 mm in diameter and 4.0 mm in length, filled with either 0.4 atm or 0.6 atm of C_5H_{12}. The diameter of the LEH was routinely 1.4 mm, with 1.2 mm and 1.8 mm also used when the effects of LEH size were explored. Each heater beam operated at 3ω with an energy of 2.2 kJ in 3 ns. Both CPP and SSD were applied, forming a focal spot of 500 μm in diameter at the LEH plane. Two beams, one from the 55° cone (A6S2) and one from the 28.5° cone (A2S2), were chosen as the LPI interaction beams, since they were equipped with backscattering diagnostic systems. To extend the intensity range, a CPP that formed a smaller (400 μm in diameter) focal spot was applied to the beam A6S2. By enhancing the energy to 3 kJ, a maximum average intensity of 1.5×10^{15} W/cm^2 was achieved.

Firstly, the effects of the interaction beam on plasma parameters were explored. The experiments were performed in the configuration of the first step with 0.4-atm hohlraums. As shown in Figs. 16 and 17, SBS and SRS spectra did not change much when the interaction beam intensity was increased from 6×10^{14} W/cm^2 to 1×10^{15} W/cm^2, which indicated that the intensity variation of a single beam had little effect on the plasma parameters inside the hohlraum. Numerical simulations performed with a combination of LARED-JC and HLIP reproduced these spectra well, demonstrating their reliability in predicting plasma parameters and LPI development at the open-end side. With the aid of numerical simulations, the detailed information of LPI development was inferred. At the beginning of the main pulse (~1–2 ns), both SBS and SRS were excited in the gas-fill region because of the low temperature inside the hohlraum, but as the plasma temperature increased, SBS and SRS were inhibited. At the end of the main pulse (~3–4 ns), the expansion of the hohlraum wall produced a large-scale Au plasma close to the wall and a high-density C_5H_{12} plasma in the gas-fill region, where SBS and SRS grew again, respectively.

Based on this platform, the dependence of SBS and SRS reflectivities on laser intensity was studied, as shown in Fig. 18. Although some shot-to-shot fluctuations existed, a clear increase in SBS and SRS reflectivities as a function of laser intensity was measured, indicating that they were generally in the linear growth regime. However, when the gas

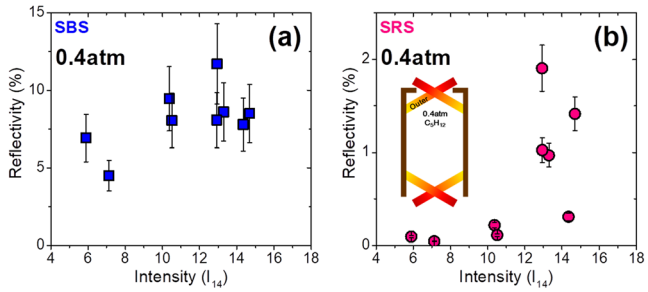

FIG. 18. Reflectivities of (a) SBS and (b) SRS as a function of interaction beam intensity in 0.4-atm hohlraums. The inset in (b) shows the sketch of the experimental setup.

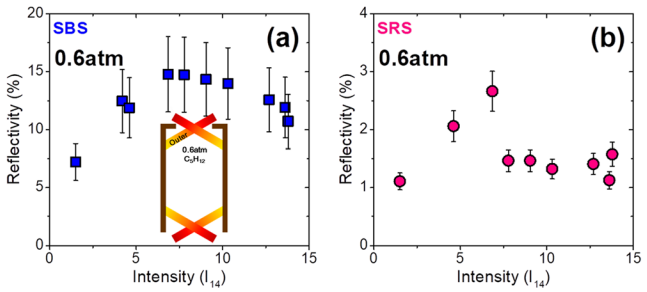

FIG. 19. Reflectivities of (a) SBS and (b) SRS as a function of interaction beam intensity in 0.6-atm hohlraums. The inset in (a) shows the sketch of the experimental setup.

pressure was enhanced from 0.4 atm to 0.6 atm, a quite different behavior was observed, as presented in Fig. 19. SBS and SRS reflectivities increased with laser intensity until ~7×10^{14} W/cm^2, and then dropped thereafter. One of the reasons might be the occurrence of nonlinear or kinetic saturation processes at high laser intensities. However, since the scattered light was just measured within the focus lens, the spray of scattered light outside the lens due to beam filamentation could be a more likely reason. For further clarification, additional diagnostic tools such as Thomson scattering and a near-backscattering diagnostic system are required, which are under implementation.

By flipping the hohlraum upside down, the effect of LEH size was explored. Because LPI primarily took place in the gas-fill region at the beginning of the main pulse, LEH size had little effect on LPI during this period, as shown by the SBS and SRS spectra from 1 ns to 2 ns in Fig. 20. However, at a later time (~3–4 ns), LEH inhibited plasma flow and hence enhanced the gas-fill density inside the laser channel. Therefore, both SBS and SRS spectra were red-shifted as LEH size decreased (see Fig. 20). LEH also caused a plasma inhomogeneity inside the laser channel at this later time. As shown in Fig. 20, both SBS and SRS spectra broadened and decayed with the reduction of LEH size. Of course, other factors could also contribute to the decay of SBS, such as the absorption of laser and scattered light inside the high-density gas-fill, as well as the reduction of Au plasma scale-length due to the inhibition of plasma flow.

When experimental results measured at this LEH side were compared with the corresponding numerical simulations, inconsistences were found. As shown in Fig. 21, both the wavelength and the intensity of SRS spectra from 3 ns to 4 ns predicted by the simulation were larger than the experimental measurements, indicating that the later-time gas-fill density at the LEH side was overestimated by the LARED-JC code. An inconsistency was also found in the SBS spectra at the open-end side. As can be seen in Fig. 16, compared with the experimental data, additional SBS spectra were observed around 2 ns. Neglect of the interpenetration between the Au and C_5H_{12} plasma at their interface could be one of the reasons. By artificially introducing some interpenetration at the interface, more consistent results were obtained.[71] These inconsistences

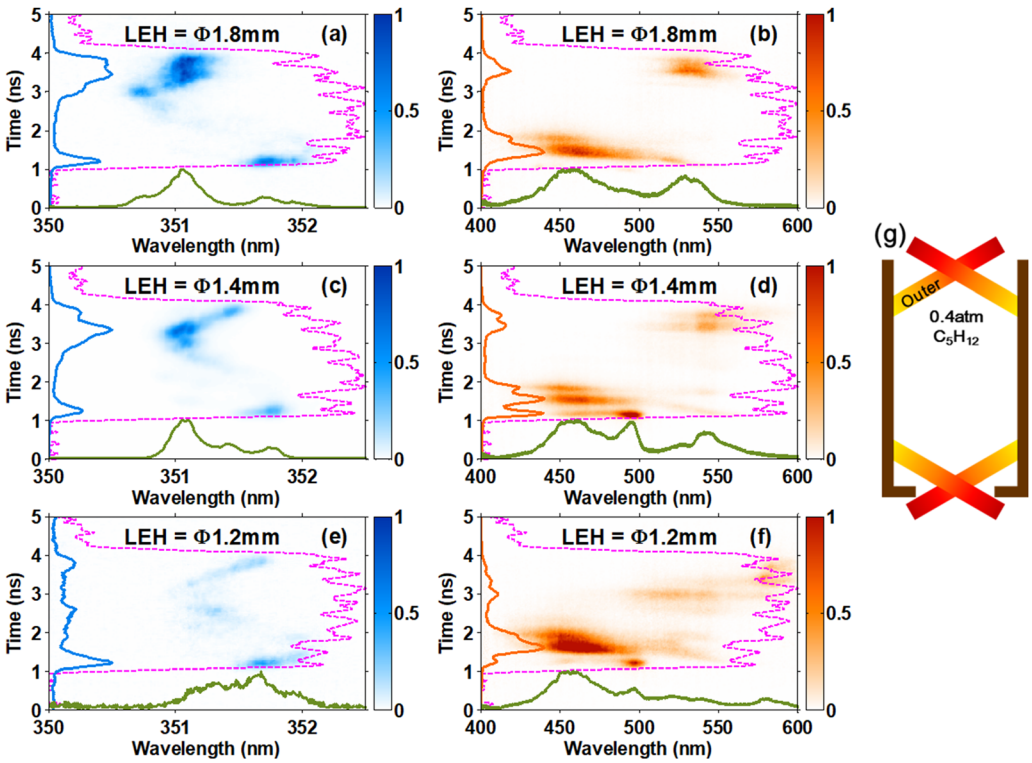

FIG. 20. (a), (c), (e) SBS and (b), (d), (f) SRS spectra measured at the LEH side in 0.4-atm hohlraums with different LEH diameters: (a), (b) 1.8 mm, (c), (d) 1.4 mm, and (e), (f) 1.2 mm. The magenta dashed lines denote the corresponding laser pulse shapes in experiments. (g) The sketch of the experimental setup.

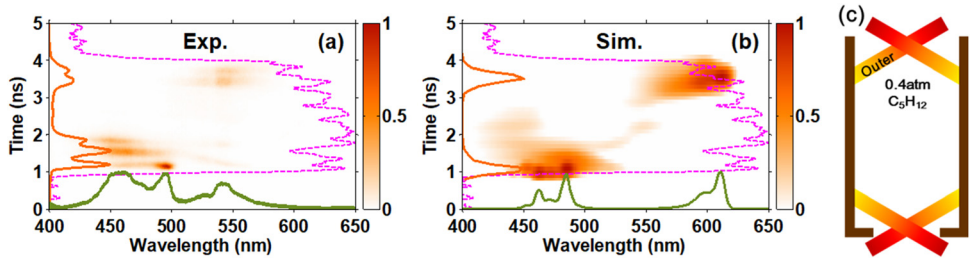

FIG. 21. (a) Experimentally measured and (b) simulated SRS spectra at the LEH side in a 0.4-atm hohlraum with LEH diameters of 1.4 mm. The laser pulse shape in the simulation is identical to the one in the experiment, as displayed by the magenta dashed lines. (c) The sketch of the experimental setup.

indicate that improvement is required in the LARED-JC code for better prediction of the hohlraum condition.

To avoid the influence of LEH and the unclear behavior of SBS and SRS reflectivities at 0.6 atm, experiments for studying the interplay between different cones of beams were performed at the open-end of a 0.4-atm hohlraum. In addition to the 32 beams from the outer cones, the 16 beams from the inner cones were also used. In these experiments, backscattering diagnostic systems were implemented on two beams: A6S2 from the outer 55° cone and A2S2 from the inner 28.5° cone. These two beams propagated in the same vertical plane, while their polarization directions were both perpendicular to the propagating plane. All of the experimental parameters were fixed except for the energy of beam A2S2. Due to the application of the additional 16 beams, a higher gas-fill temperature was achieved at the end of the main pulse; as a result, the later (~3–4 ns) component of the SRS spectra (see Fig. 22) was weaker than the corresponding result from previous experiments with 32 beams (see Fig. 17). When the energy of beam A2S2 increased from 0 J to 2.5 kJ, SBS of A6S2 remained almost constant and SRS of A6S2 was just slightly affected at a later time. Meanwhile, the behaviors of the SBS and SRS spectra of beam A2S2 were also almost independent of its energy, except for their absolute intensities. These results imply that, under the current experimental conditions, the LPI processes at different cones are generally independent, and the multi-beam LPI processes such as CBET are negligible.

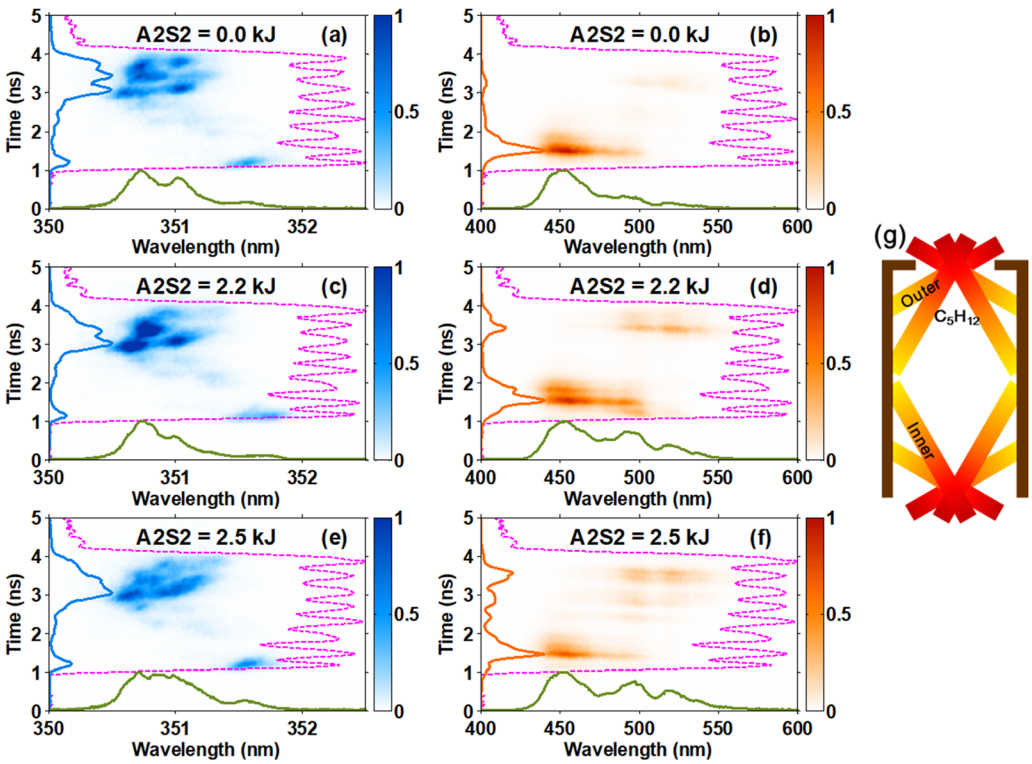

FIG. 22. (a), (c), (e) SBS and (b), (d), (f) SRS spectra from beam A6S2 with different energies of beam A2S2: (a), (b) 0 kJ, (c), (d) 2.2 kJ, and (e), (f) 2.5 kJ. The magenta dashed lines denote the corresponding laser pulse shapes in experiments. (g) The sketch of the experimental setup.

V. SUMMARY AND FUTURE WORK

During the past ten years, several series of experimental studies have been performed on the Shenguang laser facilities for LPI research. When the drive energy was limited, great efforts were made to develop large-scale plasma platforms, in which LPI could reach a high level. Millimeter scale plasmas were created in both gasbag and gas-filled hohlraum targets on SG-II. Due to the simple geometry and well-characterized plasma parameters, these platforms could play an important role in further LPI research. In later facilities which could attain larger drive energies, LPI was strong due to the simultaneous occurrence of a large-scale plasma and a high-intensity laser spot. Therefore, several beam-smoothing techniques for improving focal spot quality were intensively studied. A substantial reduction in the high-intensity component was observed with the application of CPP and PS; as a result, LPI was greatly mitigated. After the construction of SG-180 kJ, ignition-relevant conditions were achieved, which motivated research on factors affecting LPI in integrated implosion experiments. Experimental results indicate that a high-density gas-fill (e.g., 0.6 atm of C_5H_{12}) may cause beam filamentation and hence affect LPI processes. A smaller LEH would mitigate LPI at the end of the main pulse by increasing plasma inhomogeneities, although a denser gas-fill was formed due to the inhibition of plasma flow. The addition of beams in the inner cones would suppress LPI in the gas-fill region by increasing plasma temperature. Multi-beam interplay between different cones of beams has not been observed yet. All this work has greatly improved our understanding of LPI and will certainly play a significant role in future experimental design.

Obviously, more work on LPI is required and several research projects on the Shenguang laser facilities have already been proposed. For example, based on the mm-scale platform on SG-II, the effects of chirped or broadband lasers on LPI will be studied. To clarify the saturation mechanisms of SBS observed on SG-180 kJ, a similar laser and similar plasma conditions will be reproduced on SG-10 kJ, so that Thomson scattering can be used to diagnose the driven ion acoustic wave. Since the research roadmap on SG-180 kJ has not yet been completed, subsequent experiments will be conducted to uncover the impact of ablated plasma from the capsule. In addition to the square pulse used in previous LPI experiments, shaped pulses for integrated implosion experiments will also be studied.

ACKNOWLEDGMENTS

This work was supported by the Science Challenge Project (Grant No. TZ2016005), the Natural Science Foundation of China (Grant Nos. 11435011, 11875093, and 11875241), and the CAEP Foundation (Grant No. PY2019108).

REFERENCES

[1]J. D. Lindl, *Inertial Confinement Fusion: The Quest for Ignition and Energy Gain Using Indirect Drive* (Springer-Verlag, New York, 1998).

[2]J. Nuckolls, L. Wood, A. Thiessen, and G. Zimmerman, "Laser compression of matter to super-high densities: Thermonuclear (CTR) applications," Nature **239**, 139 (1972).

[3]O. A. Hurricane, D. A. Callahan, D. T. Casey, P. M. Celliers, C. Cerjan *et al.*, "Fuel gain exceeding unity in an inertially confined fusion implosion," Nature **506**, 343 (2014).

[4]I. M. Edward, "Ignition on the National ignition facility: A path towards inertial fusion energy," Nucl. Fusion **49**, 104022 (2009).

[5]W. L. Kruer, *The Physics of Laser Plasma Interactions* (Addison-Wesley, Redwood, 1988).

[6]J. D. Lindl, P. Amendt, R. L. Berger, S. G. Glendinning, S. H. Glenzer *et al.*, "The physics basis for ignition using indirect-drive targets on the National Ignition Facility," Phys. Plasmas **11**, 339 (2004).

[7]R. K. Kirkwood, B. B. Afeyan, W. L. Kruer, B. J. MacGowan, J. D. Moody *et al.*, "Observation of energy transfer between frequency-mismatched laser beams in a large-scale plasma," Phys. Rev. Lett. **76**, 2065 (1996).

[8]W. L. Kruer, S. C. Wilks, B. B. Afeyan, and R. K. Kirkwood, "Energy transfer between crossing laser beams," Phys. Plasmas **3**, 382 (1996).

[9]P. Michel, L. Divol, E. A. Williams, S. Weber, C. A. Thomas *et al.*, "Tuning the implosion symmetry of ICF targets via controlled crossed-beam energy transfer," Phys. Rev. Lett. **102**, 025004 (2009).

[10]P. Michel, L. Divol, E. A. Williams, C. A. Thomas, D. A. Callahan *et al.*, "Energy transfer between laser beams crossing in ignition hohlraums," Phys. Plasmas **16**, 042702 (2009).

[11]F. Ze, L. J. Suter, S. M. Lane, E. M. Campbell, W. C. Mead *et al.*, "Compression measurements in ablatively driven inertial confinement fusion," Comments Plasma Phys. Controlled Fusion **10**, 33 (1986).

[12]W. L. Kruer, "Intense laser plasma interactions: From Janus to Nova," Phys. Fluids B **3**, 2356 (1991).

[13]J. L. Emmett, W. F. Krupke, and J. B. Trenholme, "Future development of high-power solid-state laser systems," Sov. J. Quantum Electron. **13**, 1 (1983).

[14]J. T. Hunt and D. R. Speck, "Present and future performance of the Nova laser system," Opt. Eng. **28**, 284461 (1989).

[15]J. Bunkenberg, J. Boles, D. Brown, J. Eastman, J. Hoose *et al.*, "The omega high-power phosphate-glass system: Design and performance," IEEE J. Quantum Electron. **17**, 1620 (1981).

[16]J. Soures, R. J. Hutchison, S. D. Jacobs, L. D. Lund, R. McCrory *et al.*, *OMEGA: A Short-Wavelength Laser for Fusion Experiments* (Institute of Electrical and Electronic Engineers, New York, 1983).

[17]T. R. Boehly, D. L. Brown, R. S. Craxton, R. L. Keck, J. P. Knauer *et al.*, "Initial performance results of the OMEGA laser system," Opt. Commun. **133**, 495 (1997).

[18]E. I. Moses, R. N. Boyd, B. A. Remington, C. J. Keane, and R. Al-Ayat, "The National Ignition Facility: Ushering in a new age for high energy density science," Phys. Plasmas **16**, 041006 (2009).

[19]P. A. Holstein, D. Babonneau, C. Bowen, F. Chaland, C. Cherfils *et al.*, "Target physics for the megajoule laser (LMJ)," Nucl. Fusion **44**, S177 (2004).

[20]N. Fleurot, C. Cavailler, and J. L. Bourgade, "The laser mégajoule (LMJ) Project dedicated to inertial confinement fusion: Development and construction status," Fusion Eng. Des. **74**, 147 (2005).

[21]Z. Lin, X. Deng, D. Fan, S. Wang, S. Chen *et al.*, "SG-II laser elementary research and precision SG-II program," Fusion Eng. Des. **44**, 61 (1999).

[22]X. M. Zhang, W. G. Zheng, X. F. Wei, F. Jing, Z. Sui, *et al.*, "Preliminary experimental results of shenguang III technical integration experiment line," in *High-Power Lasers and Applications III*, edited by D. Fan, K. I. Ueda, and J. Lee (SPIE-International Society Optical Engineering, Bellingham, 2004), p. 6.

[23]W. G. Zheng, X. M. Zhang, X. F. Wei, F. Jing, Z. Sui, *et al.*, "Status of the SG-III solid-state laser facility," in *5th International Conference on Inertial Fusion Sciences and Applications*, edited by H. Azechi, B. Hammel, and J. C. Gauthier (IOP Publishing Ltd., Bristol, 2008), p. 032009.

[24]N. B. Meezan, L. J. Atherton, D. A. Callahan, E. L. Dewald, S. Dixit *et al.*, "National ignition Campaign Hohlraum energetics," Phys. Plasmas **17**, 056304 (2010).

[25]S. N. Dixit, M. D. Feit, M. D. Perry, and H. T. Powell, "Designing fully continuous phase screens for tailoring focal-plane irradiance profiles," Opt. Lett. **21**, 1715 (1996).

[26]E. Lefebvre, R. L. Berger, A. B. Langdon, B. J. MacGowan, J. E. Rothenberg *et al.*, "Reduction of laser self-focusing in plasma by polarization smoothing," Phys. Plasmas **5**, 2701 (1998).

[27]S. Skupsky, R. W. Short, T. Kessler, R. S. Craxton, S. Letzring *et al.*, "Improved laser-beam uniformity using the angular-dispersion of frequency-modulated light," J. Appl. Phys. **66**, 3456 (1989).

[28]J. D. Moody, B. J. MacGowan, J. E. Rothenberg, R. L. Berger, L. Divol *et al.*, "Backscatter reduction using combined spatial, temporal, and polarization beam smoothing in a long-scale-length laser plasma," Phys. Rev. Lett. **86**, 2810 (2001).

[29]S. H. Glenzer, R. L. Berger, L. M. Divol, R. K. Kirkwood, B. J. MacGowan *et al.*, "Reduction of stimulated scattering losses from hohlraum plasmas with laser beam smoothing," Phys. Plasmas **8**, 1692 (2001).

[30]D. H. Froula, L. Divol, R. L. Berger, R. A. London, N. B. Meezan *et al.*, "Direct measurements of an increased threshold for stimulated Brillouin scattering with polarization smoothing in ignition hohlraum plasmas," Phys. Rev. Lett. **101**, 115002 (2008).

[31]D. H. Froula, L. Divol, R. A. London, R. L. Berger, T. Doppner *et al.*, "Observation of the density threshold behavior for the onset of stimulated Raman scattering in high-temperature hohlraum plasmas," Phys. Rev. Lett. **103**, 045006 (2009).

[32]D. H. Froula, L. Divol, R. A. London, R. L. Berger, T. Doppner *et al.*, "Experimental basis for laser-plasma interactions in ignition hohlraums at the National Ignition Facility," Phys. Plasmas **17**, 056302 (2010).

[33]S. H. Glenzer, D. H. Froula, L. Divol, M. Dorr, R. L. Berger *et al.*, "Experiments and multiscale simulations of laser propagation through ignition-scale plasmas," Nat. Phys. **3**, 716 (2007).

[34]D. S. Montgomery, B. B. Afeyan, J. A. Cobble, J. C. Fernandez, M. D. Wilke *et al.*, "Evidence of plasma fluctuations and their effect on the growth of stimulated Brillouin and stimulated Raman scattering in laser plasmas," Phys. Plasmas **5**, 1973 (1998).

[35]L. F. Berzak Hopkins, N. B. Meezan, S. Le Pape, L. Divol, A. J. Mackinnon *et al.*, "First high-convergence cryogenic implosion in a near-vacuum hohlraum," Phys. Rev. Lett. **17**, 175001 (2015).

[36]D. H. Froula, J. S. Ross, B. B. Pollock, P. Davis, A. N. James *et al.*, "Quenching of the nonlocal electron heat transport by large external magnetic fields in a laser-produced plasma measured with imaging Thomson scattering," Phys. Rev. Lett. **98**, 135001 (2007).

[37]D. S. Montgomery, B. J. Albright, D. H. Barnak, P. Y. Chang, J. R. Davies *et al.*, "Use of external magnetic fields in hohlraum plasmas to improve laser-coupling," Phys. Plasmas **22**, 010703 (2015).

[38]T. Gong, J. Zheng, Z. Li, Y. Ding, D. Yang *et al.*, "Mitigating stimulated scattering processes in gas-filled hohlraums via external magnetic fields," Phys. Plasmas **22**, 092706 (2015).

[39]P. Neumayer, R. L. Berger, L. Divol, D. H. Froula, R. A. London *et al.*, "Suppression of stimulated Brillouin scattering by increased Landau damping in multiple-ion-species hohlraum plasmas," Phys. Rev. Lett. **100**, 105001 (2008).

[40]P. Neumayer, R. L. Berger, D. Callahan, L. Divol, D. H. Froula *et al.*, "Energetics of multiple-ion species hohlraum plasmas," Phys. Plasmas **15**, 056307 (2008).

[41]J. L. Kline, D. S. Montgomery, H. A. Rose, S. R. D. H. Goldman, D. H. Froula *et al.*, "Mitigation of stimulated Raman scattering in Hohlraum plasmas," in *5th International Conference on Inertial Fusion Sciences and Applications*, edited by H. Azechi, B. Hammel, and J. C. Gauthier (IOP Publishing Ltd., Bristol, 2008).

[42]C. Labaune, H. A. Baldis, B. S. Bauer, V. T. Tikhonchuk, and G. Laval, "Time-resolved measurements of secondary Langmuir waves produced by the Langmuir decay instability in a laser-produced plasma," Phys. Plasmas **5**, 234 (1998).

[43]S. Depierreux, C. Labaune, J. Fuchs, D. Pesme, V. T. Tikhonchuk *et al.*, "Langmuir decay instability cascade in laser-plasma experiments," Phys. Rev. Lett. **89**, 045001 (2002).

[44]H. C. Bandulet, C. Labaune, K. Lewis, and S. Depierreux, "Thomson-scattering study of the subharmonic decay of ion-acoustic waves driven by the Brillouin instability," Phys. Rev. Lett. **93**, 035002 (2004).

[45]C. Niemann, S. H. Glenzer, J. Knight, L. Divol, E. A. Williams *et al.*, "Observation of the parametric two-ion decay instability with Thomson scattering," Phys. Rev. Lett. **93**, 045004 (2004).

[46]D. Umstadter, R. Williams, C. Clayton, and C. Joshi, "Observation of steepening in electron plasma waves driven by stimulated Raman backscattering," Phys. Rev. Lett. **59**, 292 (1987).

[47]D. Umstadter, W. B. Mori, and C. Joshi, "The coupling of stimulated Raman and Brillouin scattering in a plasma," Phys. Fluids B **1**, 183 (1989).

[48]B. I. Cohen, B. F. Lasinski, A. B. Langdon, and E. A. Williams, "Resonantly excited nonlinear ion waves," Phys. Plasmas **4**, 956 (1997).

[49]B. I. Cohen, H. A. Baldis, R. L. Berger, K. G. Estabrook, E. A. Williams *et al.*, "Modeling of the competition of stimulated Raman and Brillouin scatter in multiple beam experiments," Phys. Plasmas **8**, 571 (2001).

[50]A. V. Maximov, W. Rozmus, V. T. Tikhonchuk, D. F. DuBois, H. A. Rose *et al.*, "Effects of plasma long-wavelength hydrodynamical fluctuations on stimulated Brillouin scattering," Phys. Plasmas **3**, 1689 (1996).

[51]S. Huller, P. E. Masson-Laborde, D. Pesme, M. Casanova, F. Detering *et al.*, "Harmonic decomposition to describe the nonlinear evolution of stimulated Brillouin scattering," Phys. Plasmas **13**, 022703 (2006).

[52]D. S. Montgomery, "Two decades of progress in understanding and control of laser plasma instabilities in indirect drive inertial fusion," Phys. Plasmas **23**, 055601 (2016).

[53]G. J. Morales and T. M. Oneil, "Nonlinear frequency-shift of an electron-plasma wave," Phys. Rev. Lett. **28**, 417 (1972).

[54]R. E. Giacone and H. X. Vu, "Nonlinear kinetic simulations of stimulated Brillouin scattering," Phys. Plasmas **5**, 1455 (1998).

[55]D. H. Froula, L. Divol, and S. H. Glenzer, "Measurements of nonlinear growth of ion-acoustic waves in two-ion-species plasmas with Thomson scattering," Phys. Rev. Lett. **88**, 105003 (2002).

[56]L. Divol, R. L. Berger, B. I. Cohen, E. A. Williams, A. B. Langdon *et al.*, "Modeling the nonlinear saturation of stimulated Brillouin backscatter in laser heated plasmas," Phys. Plasmas **10**, 1822 (2003).

[57]J. F. Myatt, J. Zhang, R. W. Short, A. V. Maximov, W. Seka *et al.*, "Multiple-beam laser-plasma interactions in inertial confinement fusion," Phys. Plasmas **21**, 055501 (2014).

[58]D. Turnbull, P. Michel, J. E. Ralph, L. Divol, J. S. Ross *et al.*, "Multibeam seeded Brillouin sidescatter in inertial confinement fusion experiments," Phys. Rev. Lett. **114**, 125001 (2015).

[59]C. Neuville, V. Tassin, D. Pesme, M. C. Monteil, P. E. Masson-Laborde *et al.*, "Experimental evidence of the collective Brillouin scattering of multiple laser beams sharing acoustic waves," Phys. Rev. Lett. **116**, 235002 (2016).

[60]D. E. Hinkel, M. D. Rosen, E. A. Williams, A. B. Langdon, C. H. Still *et al.*, "Stimulated Raman scatter analyses of experiments conducted at the National Ignition Facility," Phys. Plasmas **18**, 056312 (2011).

[61]P. Michel, L. Divol, E. L. Dewald, J. L. Milovich, M. Hohenberger *et al.*, "Multi-beam stimulated Raman scattering in inertial confinement fusion conditions," Phys. Rev. Lett. **115**, 055003 (2015).

[62]C. Stoeckl, R. E. Bahr, B. Yaakobi, W. Seka, S. P. Regan *et al.*, "Multibeam effects on fast-electron generation from two-plasmon-decay instability," Phys. Rev. Lett. **90**, 235002 (2003).

[63]E. L. Dewald, F. Hartemann, P. Michel, J. Milovich, M. Hohenberger *et al.*, "Generation and beaming of early hot electrons onto the capsule in laser-driven ignition hohlraums," Phys. Rev. Lett. **116**, 075003 (2016).

[64]Z. C. Li, J. Zheng, X. H. Jiang, Z. B. Wang, D. Yang *et al.*, "Interaction of 0.53 μm laser pulse with millimeter-scale plasmas generated by gasbag target," Phys. Plasmas **19**, 062703 (2012).

[65]Z. C. Li, J. Zheng, X. H. Jiang, Z. B. Wang, D. Yang *et al.*, "Methods of generation and detailed characterization of millimeter-scale plasmas using a gasbag target," Chin. Phys. Lett. **28**, 125202 (2011).

[66]Z. B. Wang, J. Zheng, B. Zhao, C. X. Yu, X. H. Jiang *et al.*, "Thomson scattering from laser-produced gold plasmas in radiation conversion layer," Phys. Plasmas **12**, 082703 (2005).

[67]Z. C. Li, J. A. Zheng, Y. K. Ding, Q. A. Yin, X. H. Jiang *et al.*, "Generation and characterization of millimeter-scale plasmas for the research of laser plasma interactions on Shenguang-III prototype," Chin. Phys. B **19**, 125202 (2010).

[68]L. Hao, Y. Q. Zhao, D. Yang, Z. J. Liu, X. Y. Hu *et al.*, "Analysis of stimulated Raman backscatter and stimulated Brillouin backscatter in experiments performed on SG-III prototype facility with a spectral analysis code," Phys. Plasmas **21**, 072705 (2014).

[69]T. Gong, Z. Li, B. Zhao, G.-y. Hu, and J. Zheng, "Noise sources and competition between stimulated Brillouin and Raman scattering: A one-dimensional steady-state approach," Phys. Plasmas **20**, 092702 (2013).

[70]H. Yong, P. Song, C.-L. Zhai, D.-G. Kang, J.-F. Gu *et al.*, "Numerical simulation of 2-D radiation-drive ignition implosion process," Commun. Theor. Phys. **59**, 737 (2013).

[71]L. Hao, D. Yang, X. Li, Z. Li, Y. Liu *et al.*, "Laser plasma instability studies in the context of six-side laser-driven indirect designs on SG-III laser facility," Phys. Plasmas (submitted).